# Finite Element Analysis for Linear Elastic Solids Based on Subdivision Schemes*

**Daniel Burkhart[1], Bernd Hamann[2], and Georg Umlauf[3]**

1 **University of Kaiserslautern**
burkhart@cs.uni-kl.de
2 **University of California, Davis**
hamann@cs.ucdavis.edu
3 **HTWG Konstanz**
umlauf@htwg-konstanz.de

**Abstract**

Finite element methods are used in various areas ranging from mechanical engineering to computer graphics and bio-medical applications. In engineering, a critical point is the gap between CAD and CAE. This gap results from different representations used for geometric design and physical simulation.

We present two different approaches for using subdivision solids as the only representation for modeling, simulation and visualization. This has the advantage that no data must be converted between the CAD and CAE phases. The first approach is based on an adaptive and feature-preserving tetrahedral subdivision scheme. The second approach is based on Catmull-Clark subdivision solids.

**Keywords and phrases** Subdivision solids, Finite element method, Isogeometric analysis

**Digital Object Identifier** 10.4230/OASIcs.VLUDS.2010.1

## 1 Introduction

In engineering, one of the major problems is still the gap between computer-aided design (CAD) and computer-aided engineering (CAE). This gap results from different representations used for the design based on exact geometries, like boundary representations (B-Reps) or non-uniform rational B-splines (NURBS), and for the simulation based on approximative mesh representations.

As illustrated in Figure 1, design and analysis are typically done sequentially or iteratively in multiple design-simulation loops. In the initial CAD modeling and CAE pre-processing phases the boundary surface is modeled, the interior of the model is meshed and the boundary conditions, such as external forces, are defined. As the CAD and CAE model have different representations, in general a time consuming data conversion between the CAD and CAE system is required. This step also causes additional approximation errors. In the subsequent CAE processing phase the resulting system of equations is solved and in the CAE post-processing phase the solution is analyzed. If the simulation results are inadequate the geometric model can be adapted or the mesh can be refined to increase the accuracy of the

* This research was supported by the German Research Foundation (DFG), which has provided the funds for the International Research Training Group (IRTG) 1131, entitled 'Visualization of Large and Unstructured Data Sets'. We gratefully acknowledge DFG's support, and also thank our colleagues from the AG Computergrafik at the University of Kaiserslautern and the Institute for Data Analysis and Visualization (IDAV) at the University of California, Davis, for their many valuable comments.





simulation. This might also require a time consuming and approximating data conversion. These optional, iterative steps are marked as dashed arrows in Figure 1.

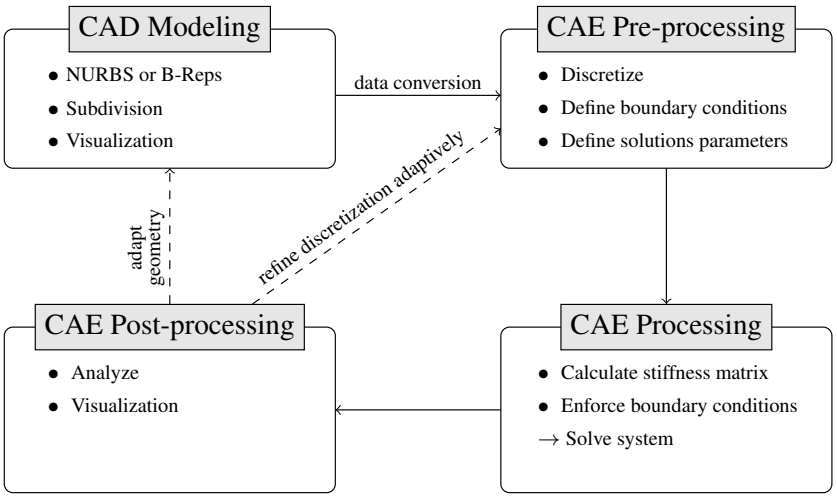


**Figure 1** Different phases in the modeling and simulation process.

One solution to this time-consuming task is iso-geometric analysis (IGA), see [14]. The idea of this approach is to extend the finite element method such that it can also handle exact geometries. Thus, there is no need to transform the geometries to mesh representations which guarantees a seamless integration of CAD and CAE. Originally, IGA was based on NURBS, see [13]. Meanwhile, similar approaches for other geometric descriptions like B-Splines [17], T-Splines [1], or subdivision surfaces [10, 11] were presented. An important aspect of IGA is the fact that refinement or degree elevation of the exact geometric model can be used to increase the simulation accuracy without changing the geometry.

In this paper, we present two approaches based on subdivision solids. This extends the idea of IGA to unstructured, refinable volumetric meshes of arbitrary topology. The first approach is based on tetrahedral subdivision inspired by $\sqrt{3}$-subdivision for surfaces. This approach supports adaptive refinement and sharp features. The second approach is based on a hexahedral subdivision scheme, which generalizes Catmull-Clark subdivision surfaces to solids. This approach uses the same basis functions for the representation of the geometry and for the integration of elements during the simulation.

In Sections 2 and 3 we review subdivision surfaces and solids. Standard finite element techniques for linear elasticity problems are described in Section 4. In Sections 5 and 6 we describe two approaches for finite element analysis based on subdivision solids.

## 2 Subdivision surfaces

Subdivision surfaces are a powerful tool to model free-form surfaces of arbitrary topology. A subdivision surface is defined as the limit of an iterative refinement process starting with a polygonal base mesh $M_0$ of control points. Iterating the subdivision process generates a sequence of refined meshes $M_1, \ldots, M_n$, that converges to a smooth limit surface $M_\infty$ for $n \to \infty$. Usually the subdivision operator can be factored into a topological refinement operation followed by a geometrical smoothing operation. While the topological refinement

inserts new vertices or flips edges, the geometrical smoothing changes vertex positions. To enforce and preserve sharp features such as corners and creases, special subdivision rules can be defined. Examples for such special rules, where tagged edges will yield creases on the subdivision surface, are presented in [15, 5, 23].

Subdivision surfaces either approximate or interpolate the base mesh. For approximating schemes the control points of $M_i$ usually do not lie on $M_{i+1}$, $i \geq 0$. The Catmull-Clark algorithm [7] is an examples of such a scheme. Approximating schemes for arbitrary triangle meshes are the Loop algorithm and $\sqrt{3}$-subdivision [19, 18]. The corresponding topological refinement operators are illustrated in Figure 2. For interpolating schemes all control points of $M_i$ are also in $M_{i+1}$, $i \geq 0$. Thus, the limit surface interpolates these points. The earliest interpolating subdivision scheme for surfaces is the butterfly scheme of [12]. For further details on subdivision surfaces refer to [21].

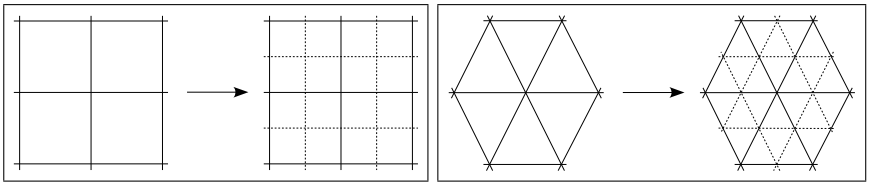

**(a)** Catmull-Clark subdivision. **(b)** Loop subdivision.

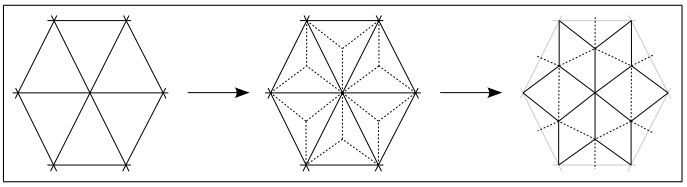

**(c)** $\sqrt{3}$ subdivision.

**Figure 2** Topological refinement operators.

## 3 Subdivision solids

Like subdivision surfaces, subdivision solids are defined as the limit of an iterative refinement process, factored into topological and geometrical refinement operations. One of the first solid subdivision schemes is described in [16]. This is a generalization of Catmull-Clark subdivision to three-dimensional solids for smooth deformations based on unstructured hexahedral meshes. As the topological refinement operation of this algorithm made it hard to analyze the smoothness of the resulting limit solid a modified operation was proposed in [6]. The advantage of this scheme is its simplicity compared to the other subdivision solids, e.g. [8, 9, 20]. From a hexahedral base mesh, only hexahedral elements are generated, all inserted vertices are regular, i.e., they have valence six, and the limit solids are at least $C^1$ away from creases or corners. The subdivision rules for Catmull-Clark solids for hexahedral meshes are defined by five steps:

1. For each hexahedron with nodes $V_1, \ldots, V_8$ add a cell point $C = (V_1 + \cdots + V_8)/8$.
2. For each face add a face point $F = (C_0 + 2A + C_1)/4$, where $C_0$ and $C_1$ are the cell points of the two incident hexahedra and $A$ is the face centroid.
3. For each edge add an edge point $E = (C_{\text{avg}} + 2A_{\text{avg}} + (n-3)M)/n$, where $n$ is the number of incident faces, $M$ is the edge midpoint, and $C_{\text{avg}}$ and $A_{\text{avg}}$ are the averages of

cell and face points of incident cells and faces, respectively.

4. For each hexahedron connect its cell point to all its face points and connect all face points to all incident edge points. This splits one hexahedron into eight hexahedra.
5. Move each original vertex $V_{\text{old}}$ to $V_{\text{new}} = (C_{\text{avg}} + 3A_{\text{avg}} + 3M_{\text{avg}} + V_{\text{old}})/8$, where $C_{\text{avg}}$, $A_{\text{avg}}$, and $M_{\text{avg}}$ are the averages of the cell, face and edge points of all adjacent cells, faces, and edges, respectively.

For faces, edges and vertices on the boundary of the solid corresponding rules for Catmull-Clark surfaces are applied.

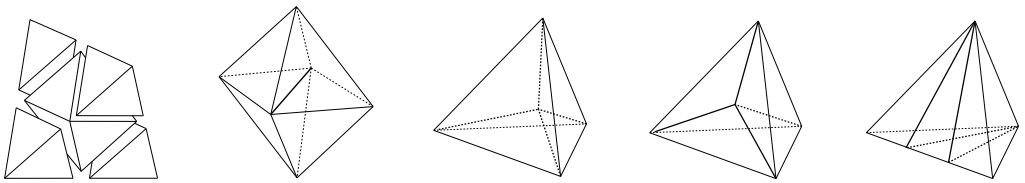

**(a)** Edge bisection. **(b)** Diagonal in octahedron. **(c)** 1-4 split. **(d)** 1-3 split. **(e)** Edge trisection.

**Figure 3** Split operations for tetrahedral subdivision.

A subdivision scheme for tetrahedral meshes based on trivariate box splines was proposed in [8, 9]. This scheme is approximating or interpolating depending on the geometrical smoothing operation. The topological refinement first splits every tetrahedron into four tetrahedra and one octahedron. This operations is illustrated in Figure 3a. Subsequently, every octahedron is split along one of its diagonals into four tetrahedra causing a potential directional bias as shown in Figure 3b.

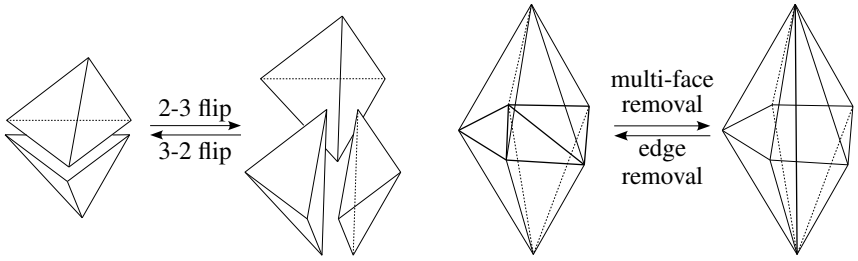


**(a)** 2-3 and 3-2 flip operation. **(b)** Multi-face removal and edge removal.

**Figure 4** Flip operations for tetrahedral subdivision.

In [2] another tetrahedral subdivision scheme that generalizes the idea of $\sqrt{3}$ subdivision [18] for triangular meshes is described. While $\sqrt{3}$ subdivision is based on triangular 1-3 splits and edge flips, this tetrahedral subdivision scheme is a combination of 1-4 splits (Figure 3c) and 2-3 flips (Figure 4a) in the interior and the $\sqrt{3}$ scheme and edge removals (Figure 4b) on the boundary. For these boundary steps, tetrahedral 1-3 splits (Figure 3d) are required. For preservation of sharp features 1-3 edge splits (Figure 3e) are required. Additional optimization steps are used to guarantee high quality of the tetrahedra. In contrast to earlier solid subdivision schemes, this scheme allows for adaptive refinement by restricting the 2-3 flips and the boundary edge removals, control of the shape of the tetrahedra by adjusting the optimization steps, and preservation of sharp features by adjusting the two

smoothing operations. The latter can also be used to replace the original $\sqrt{3}$ smoothing by an interpolatory smoothing. These properties make this subdivision scheme suitable for FEM simulations. For details see [2].

## 4 Finite element analysis of linear elastic solids

Finite element analysis is a numerical method to solve partial differential equations by first discretizing these equations in their spatial dimensions. This discretization is done locally in small regions of simple shape (the finite elements) connected at discrete nodes. The solution of the variational equations is approximated with local shape functions defined for the finite elements.

For volumetric problems the most common element types are hexahedra and tetrahedra. Typically, these elements are defined in a local coordinate system. This simplifies the construction of shape functions also for higher-order elements with curved boundaries and the numerical quadrature arising during the assembly of the stiffness matrix. If the same shape functions are used to describe the variation of the unknowns, such as displacement or fluid potential, and the mapping between the global and local coordinates, the elements are called iso-parametric elements.

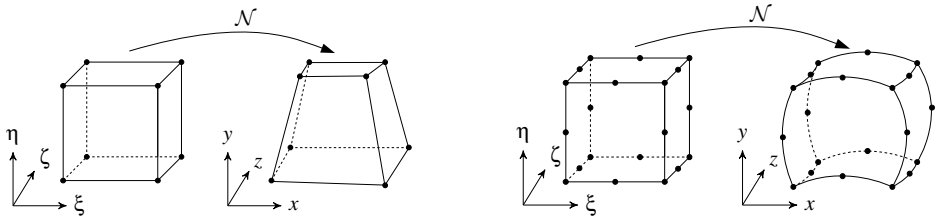


**(a)** Tri-linear hexahedral element **(b)** Tri-quadratic hexahedral element

**Figure 5** Lagrangian hexahedral elements. Both elements are shown in local and global coordinates related by the corresponding shape functions $\mathcal{N}$.

A tri-linear and a tri-quadratic hexahedral element are illustrated in Figure 5, where $(\xi, \eta, \zeta)$ are local and $(x, y, z)$ are global coordinates. The tri-linear element, for instance, has eight local shape functions $\mathcal{N} = [\mathcal{N}_1, ..., \mathcal{N}_8]$ defined over the cube $[-1, +1]^3$. For more details on elements of different order and their shape functions refer to [22].

The finite element approximation results in matrix equations relating the input (boundary conditions) at the discrete nodes to the output at these same nodes (the unknown variables). The contribution of each element is computed in terms of local stiffness matrices $\mathbf{K}_m$, which are assembled into a global stiffness matrix $\mathbf{K}$. This yields for static elasticity problems a linear system of equations $\mathbf{Ku} = \mathbf{f}$, where $\mathbf{u}$ is the vector of the unknown variables and $\mathbf{f}$ if the vector of external forces.

During the assembly of the stiffness matrix the shape functions and their derivatives with respect to global coordinates are involved. To convert these derivatives between the coordinate systems the Jacobian matrix given by

$$\mathbf{J} = \begin{bmatrix} \partial x/\partial \xi & \partial y/\partial \xi & \partial z/\partial \xi \\ \partial x/\partial \eta & \partial y/\partial \eta & \partial z/\partial \eta \\ \partial x/\partial \zeta & \partial y/\partial \zeta & \partial z/\partial \zeta \end{bmatrix}.$$

is used. For a linear elastic body $\Omega$, the equations for the computation of $\mathbf{K}_m$ are typically

derived from the strain energy defined as

$$E_{\text{strain}} = \frac{1}{2}\int_{\Omega} \epsilon^T \sigma \, d\mathbf{x},$$

with the stress vector $\sigma$ and the strain vector $\epsilon = [\epsilon_x \ \epsilon_y \ \epsilon_z \ \gamma_{xy} \ \gamma_{xz} \ \gamma_{yz}]^T$ defined as

$$\begin{aligned} &\epsilon_x = \partial u/\partial x, && \epsilon_y = \partial u/\partial y, && \epsilon_z = \partial u/\partial z, \\ &\gamma_{xy} = \partial u/\partial y + \partial v/\partial x, && \gamma_{xz} = \partial u/\partial z + \partial w/\partial x, && \gamma_{yz} = \partial v/\partial z + \partial w/\partial y. \end{aligned}$$

This can be rewritten as $\epsilon = \mathbf{B}u$, where $\mathbf{B}$ is the strain-displacement matrix.

$$\mathbf{B}^T = \begin{bmatrix} \partial/\partial x & 0 & 0 & \partial/\partial y & \partial/\partial z & 0 \\ 0 & \partial/\partial y & 0 & \partial/\partial x & 0 & \partial/\partial z \\ 0 & 0 & \partial/\partial z & 0 & \partial/\partial x & \partial/\partial y \end{bmatrix}.$$

Hooke's law $\sigma = \mathbf{C}\epsilon$ relates the stress vector $\sigma$ to $\epsilon$ via the material matrix $\mathbf{C}$. For homogeneous, isotropic material $\mathbf{C}$ is defined by the Lamé constants $\lambda$ and $\mu$, and

$$\mathbf{C} = \begin{bmatrix} \lambda+2\mu & \lambda & \lambda & 0 & 0 & 0 \\ \lambda & \lambda+2\mu & \lambda & 0 & 0 & 0 \\ \lambda & \lambda & \lambda+2\mu & 0 & 0 & 0 \\ 0 & 0 & 0 & \mu & 0 & 0 \\ 0 & 0 & 0 & 0 & \mu & 0 \\ 0 & 0 & 0 & 0 & 0 & \mu \end{bmatrix}.$$

Rewriting the strain energy and adding work applied by eternal forces $\mathbf{f}$ to the boundary $\Gamma$, yields the total energy function

$$E(\mathbf{u}) = \frac{1}{2}\int_{\Omega} \mathbf{u}^T\mathbf{B}^T\mathbf{C}\mathbf{B}\,\mathbf{u}\, d\mathbf{x} - \int_{\Gamma} \mathbf{f}^T\mathbf{u}\, d\mathbf{x}. \tag{1}$$

This energy function can be approximated with finite elements in terms of

$$\mathbf{K}_m = \iiint \mathbf{B}^T\mathbf{C}\mathbf{B}\, dx\, dy\, dz. \tag{2}$$

As the exact evaluation of (2) is in general not possible Gauss quadrature is used

$$\int_{-1}^{+1}\int_{-1}^{+1}\int_{-1}^{+1} \mathbf{f}(x,y,z)dxdydz \approx \sum_{i=1}^{n} W_i \mathbf{f}(x_i,y_i,z_i), \tag{3}$$

where $x_i$, $y_i$ and $z_i$ are the sampling points of the univariate quadrature rule and $W_i$ is the product of the corresponding weights. As the elements are defined in local coordinates, combining (3) with (2) yields

$$\mathbf{K}_m \approx \sum_{i=1}^{n} W_i \det(\mathbf{J})\mathbf{B}^T\mathbf{C}\mathbf{B}, \tag{4}$$

where the Jacobian matrix $\mathbf{J}$ and $\mathbf{B}$ are evaluated at the sampling points. This requires evaluating the derivatives of the shape functions, see [24, 22] for details.

## 5 Adaptive tetrahedral subdivision for finite element analysis

In [3] we demonstrate the effectiveness of adaptive and feature-preserving tetrahedral subdivision for finite element simulations for the engineering part shown in Figure 6 (top left

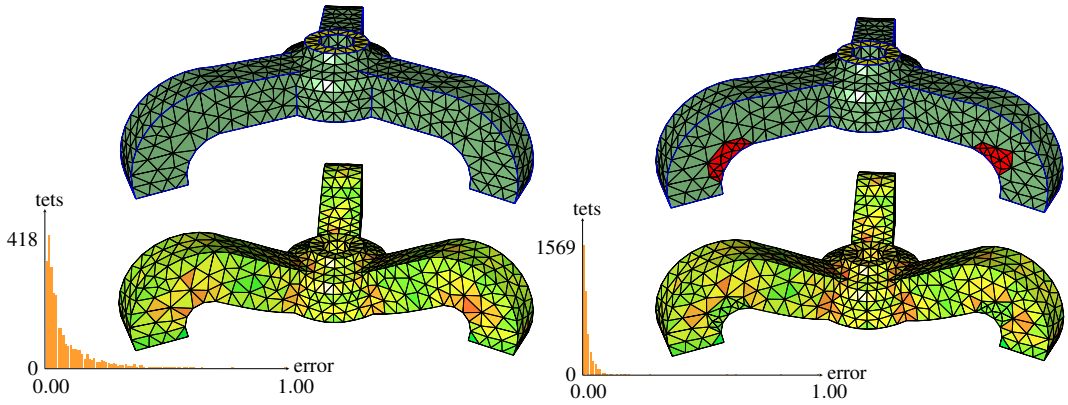


**Figure 6** Adaptive subdivision and FE simulation. First column: tetrahedral base mesh (2,799 tetrahedra) and simulation with visualization of the approximation error (green=low – red=high) and the histogram of the error distribution; second column: adaptively refined mesh (4,540 tetrahedra) showing the refined regions in red, and simulation results for the once adaptively refined mesh.

model) consisting of 2,799 tetrahedra. To the top faces (yellow) of the tripod a vertical load is applied and the bottom of the legs of the tripod are fixed.

Figure 6 (bottom left model) visualizes the normalized approximation error of the deformed model, where the color hue is linearly interpolated from 0° (low error) to 120° (high error). The simulation took 491ms while the average normalized error is 0.08. The histogram shows the error distribution for the tetrahedra.

For the next step the mesh regions with the largest error are selected and refined. These refined regions are highlighted in red in Figure 6 (top right model). As some of these regions are isolated, one round of region growing is used to decrease the number of disconnected, refined regions. The adaptively refined mesh consists of 4,540 tetrahedra. Figure 6 (bottom right model) shows the deformation of this new tetrahedral mesh. The simulation took 596ms while the average normalized error is 0.03. Without adaptive refinement the mesh consists of 23,480 tetrahedra after one subdivision step. This yields a simulation time of 7,574ms with average normalized error 0.008 for the globally refined mesh. The decrease of error and the histograms getting narrower demonstrates that our method is effective. The efficiency of the proposed methods is demonstrated by reducing the computation times by a factor of twelve for the adaptively refined mesh compared to the globally refined meshes. For more details see [3].

## 6 Hexahedral finite element analysis based on Catmull-Clark solids

For the method presented in Section 5, tetrahedral subdivision was used to represent the geometry and to adaptively refine the mesh, but for the analysis, standard linear Lagrangian tetrahedral elements are used. In [4] we described a method that uses Catmull-Clark solids for the representation of the geometry and the approximation of the displacement field defined by Equation (1).

The major problem with this method is that the displacement field within an element does not only depend on the displacements of the nodes attached to the element but also on the displacements of the nodes of adjacent elements, because the support of the basis functions of Catmull-Clark solids overlaps a one-ring neighborhood of elements. This is

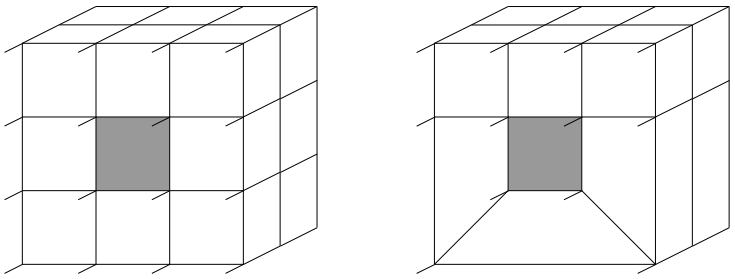

**(a)** Regular Catmull-Clark element

**(b)** Irregular Catmull-Clark element

**Figure 7** To evaluate the highlighted hexahedron, all adjacent hexahedra are required.

illustrated in Figure 7, where the gray element is evaluated, but adjacent elements are also required to evaluate the derivatives in Equation (4).

For standard tri-linear and tri-quadratic elements these derivatives can be computed directly. For Catmull-Clark elements it is not obvious how to compute derivatives due to topologically arbitrary elements as shown in Figure 7b. However, evaluating the topological arbitrary elements can be reduced to evaluations of regular elements shown in Figure 7a. These regular elements can be evaluated directly with B-spline basis functions, since Catmull-Clark solids are generalizations of tri-variate cubic B-splines. For details on how to evaluate irregular elements see [4].

To demonstrate the effectiveness of our approach, we compare it to standard finite elements shown in Figure 5. As a test case we use the model shown in Figure 8a. This model is fixed at the left and right side, and a vertical load is applied to the top. We measure the maximum displacement in the direction of the load. Compared to standard tri-linear and tri-quadratic hexahedral elements Catmull-Clark elements converge faster to a reference solution. Furthermore, Catmull-Clark elements are numerically more stable than tri-quadratic finite elements. It seems that Catmull-Clark elements produce a more homogeneous stiffness matrix, which results in faster solution of the linear system of equations and in better conditioned stiffness matrices.

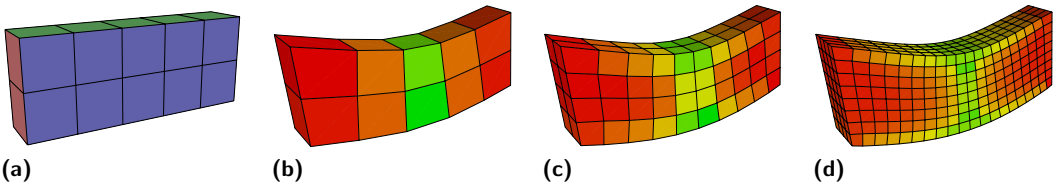


**Figure 8** (a) Base mesh of model to be simulated. Red faces are fixed, to green faces a load is applied. (b) Simulation of base mesh, (c) simulation of once refined mesh, (d) simulation of twice refined mesh. For the visualization of the stress the same scale is used as in Figure 6.

Our approach is also applicable to unstructured meshes with irregular vertices and large, real-world examples. Figure 9 shows a simulation where a mesh with interior irregular vertices of valence six and ten is rotated. For the simulation, the red faces are fixed and for the vertices at the opposite side a fixed displacement is computed. Fore more examples and details concerning the convergence analysis see [4].

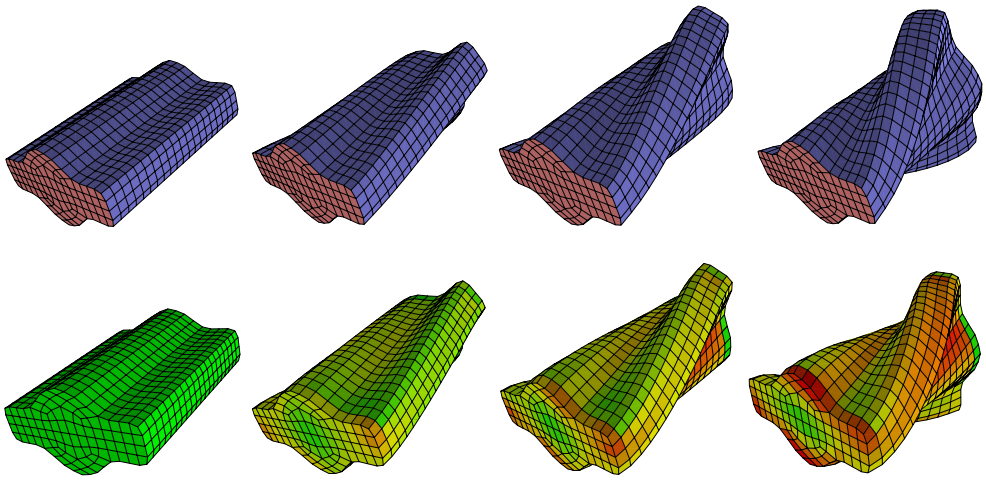

**Figure 9** Simulated rotation of a model with interior vertices of valence six and ten. For the visualization of the stress the same scale is used as in Figure 6.

## 7 Conclusion and future work

In this paper we have presented two approaches for combining solid subdivision and FE analysis. The major advantage of these approaches is that only one representation is used for modeling, visualization and simulation of solid models, by means of an adaptive tetrahedral subdivision tailored for FE applications and an iso-geometric approach for finite element analysis based on Catmull-Clark solids.

For the future we plan to combine these subdivision schemes with more complex FE models, e.g. non-linear deformations and problems from fluid dynamics. For the second method only hexahedral meshes are supported but we are working on generalizations to arbitrary polyhedral meshes. Here, the evaluation technique of [4] can be generalized to the adaptive tetrahedral subdivision scheme presented in [2].

## References


1 Y. Bazilevs, V.M. Calo, J.A. Cottrell, J.A. Evans, T.J.R. Hughes, S. Lipton, M.A. Scott, and T.W. Sederberg. Isogeometric analysis using T-splines. *Comp. Meth. in Applied Mech. and Eng.*, 199(5-8):229 – 263, 2010.

2 D. Burkhart, B. Hamann, and G. Umlauf. Adaptive and Feature-Preserving Subdivision for High-Quality Tetrahedral Meshes. *Comput. Graph. Forum*, 29(1):117–127, 2010.

3 D. Burkhart, B. Hamann, and G. Umlauf. Adaptive tetrahedral subdivision for finite element analysis. In *Comput. Graph. International, Electronic Proceedings*, 2010.

4 D. Burkhart, B. Hamann, and G. Umlauf. Iso-geometric Finite Element Analysis Based on Catmull-Clark Subdivision Solids. *Proceedings of Symposium on Geometry Processing, Computer Graphics Forum*, 29(5):1575–1584, 2010.

5 Henning Biermann, Ioana M. Martin, Denis Zorin, and Fausto Bernardini. Sharp features on multiresolution subdivision surfaces. *Graph. Models*, 64(2):61–77, 2002.

6 C. Bajaj, S. Schaefer, J. Warren, and G. Xu. A subdivision scheme for hexahedral meshes. *The Visual Computer*, 18:343–356, 2002.

7 E. Catmull and J. Clark. Recursively generated B-spline surfaces on arbitrary topological meshes. *Computer-Aided Design*, 10(6):350–355, 1978.

**8** Yu-Sung Chang, Kevin T. McDonnell, and Hong Qin. A new solid subdivision scheme based on box splines. In *Proc. 7th ACM Symp. on Solid Modeling and Appl.*, pages 226–233, 2002.

**9** Yu-Sung Chang, Kevin T. McDonnell, and Hong Qin. An Interpolatory Subdivision for Volumetric Models over Simplicial Complexes. In *Proc. Shape Modeling International*, pages 143–152, 2003.

**10** Fehmi Cirak, Michael Ortiz, and Peter Schröder. Subdivision Surfaces: A New Paradigm For Thin-Shell Finite-Element Analysis. *Int. J. Num. Meth. Eng.*, 47:2039–2072, 2000.

**11** Fehmi Cirak, Michael J. Scott, Erik K. Antonsson, Michael Ortiz, and Peter Schröder. Integrated Modeling, Finite-Element Analysis, and Engineering Design for Thin-Shell Structures using Subdivision. *Computer-Aided Design*, 34:137–148, 2002.

**12** Nira Dyn, David Levine, and John A. Gregory. A butterfly subdivision scheme for surface interpolation with tension control. *ACM Trans. Graph.*, 9(2):160–169, 1990.

**13** G. Farin. *Curves and Surfaces for CAGD: A Practical Guide*. Morgan Kaufmann, 5th edition, 2001.

**14** T. J. R. Hughes, J. A. Cottrell, and Y. Bazilevs. Isogeometric analysis: CAD, finite elements, NURBS, exact geometry and mesh refinement. *Comp. Meth. in Applied Mech. and Eng.*, 194(39-41):4135–4195, 2005.

**15** Hugues Hoppe, Tony DeRose, Tom Duchamp, Mark Halstead, Hubert Jin, John McDonald, Jean Schweitzer, and Werner Stuetzle. Piecewise smooth surface reconstruction. In *Proceedings of SIGGRAPH*, pages 295–302, 1994.

**16** K. Joy and R. MacCracken. The refinement rules for Catmull-Clark solids. *Technical Report 96-1*, UC Davis, 1996.

**17** Pavel Kagan, Anath Fischer, and Pinhas Z. Bar-Yoseph. Integrated mechanically based CAE system. In *ACM Symposium on Solid modeling and applications*, pages 23–30, 1999.

**18** L. Kobbelt. $\sqrt{3}$ Subdivision. In *Proceedings of SIGGRAPH*, pages 103–112, 2000.

**19** C. Loop. Smooth Subdivision Surfaces Based on Triangles. *Master's thesis, University of Utah*, 1987.

**20** Valerio Pascucci. Slow growing volumetric subdivision. In *Proceedings of SIGGRAPH*, pages 251–251, 2002.

**21** J. Peters and U. Reif. *Subdivision Surfaces*. Springer, 2008.

**22** I. Smith and D. Griffiths. *Programming the Finite Element Method*. Wiley, 2004.

**23** J. Warren and H. Weimer. *Subdivision Methods for Geometric Design*. Morgan Kaufmann Publishers, 2002.

**24** O.C. Zienkiewicz and R.L. Taylor. *The Finite Element Method, Volume 1+2*. Butterworth, 5th edition, 2000.